The wheat VIH2-3B, a functional PPIP5K controls the localization of fasciclin-like arabinogalactan protein

Author names and affiliations:

Anuj Shukla[1,2,3], Rahul Tanwar[1,4], Kanupriya Agrwal[1], Riya Ghosh[5], Henning Jacob Jessen[2,3], Debabrata Laha[5] and Ajay K Pandey[1,*]

[1]National Agri-Food Biotechnology Institute (Department of Biotechnology), Sector 81, Knowledge City, S.A.S. Nagar, Punjab, India.

[2] Institute of Organic Chemistry, University of Freiburg, Albertstraße 21, 79104, Freiburg, Germany.

[3]CIBSS - Centre for Integrative Biological Signalling Studies, University of Freiburg, 79104 Freiburg, Germany.

[4]Regional Centre for Biotechnology, Faridabad - 121001 Haryana (NCR), Delhi, India

[5]Department of Biochemistry, Indian Institute of Science, Bengaluru-560012, Karnataka, India

**Corresponding author:*

Dr. Ajay K Pandey, Scientist-F

Email: pandeyak@nabi.res.in; pandeyak1974@gmail.com

ORCID iD: https://orcid.org/0000-0003-1064-139X

Abstract

Inositol pyrophosphates (PP□InsPs) are important signalling molecules, that participate in multiple physiological processes across a wide range of eukaryotes. Metabolic pathway kinases (VIP1/VIHs) leading to the production of PP-InsPs are now well characterized in yeast and plants. Previously, the wheat inositol pyrophosphate kinase (*TaVIH2*) was shown to encode a catalytic active kinase domain. Heterologousexpression of *TaVIH2* in *Arabidopsis thaliana* showed enhanced drought tolerance by modulating the cell composition. In this study, we attempted to identify the interacting protein targets of wheat VIH2-3B using a yeast two-hybrid (Y2H) cDNA library screen, identifying 52 putative interactors that are primarily involved in cell wall-related functions. Notably, fasciclin-like arabinogalactan protein (FLA7), a glycosylphosphatidylinositol (GPI)-anchored protein emerged as the most frequently interacting partner in the screen. Further analysis using pull-down assays validated the interaction between TaVIH2-3B and TaFLA7 *in vivo*. Using the reporter fusion studies, we observed the localization of TaFLA7 to be a plasma membrane. We also observed that this localization of the FLA7 was perturbed in the yeast *vip1*Δ strain. The expression of TaVIH2-3B bearing PP-InsP5K enzymatic activity in yeast mutants rescued the localisation of the FLA7 to the membrane. Expression analysis of *TaFLA7* showed differential expression response under drought in wheat shoot tissues. *TaFLA7* was also found to be highly expressed during grain development, particularly in the endosperm and seed coat during grain maturation. Taken together, these findings highlight the potential role of TaVIH2 in cell wall remodelling and stress response pathways, offering new insights into the functional roles of VIH proteins in plants.

Key word: Inositol pyrophosphates, kinases, cell wall maintenance.

Introduction

Inositol pyrophosphates (PP-InsPs) are high-energy molecules that are ubiquitous in various eukaryotic organisms and serve as critical cellular signaling entities(Zsolt et al. 2011). Over the last two decades, inositol pyrophosphate signalling has gained significant attention and proven to regulate different cellular functions such as regulating telomere length, DNA repair, phosphate homeostasis, vesicular trafficking and protein phosphorylation (Saiardi 2004; Fridy et al. 2007; Lee et al. 2007; Azevedo et al. 2009; Thota and Bhandari 2015; Shears 2015; Sanchez et al. 2019; Pipercevic et al. 2023; Chabert et al. 2023). Researchers have identified two distinct classes of inositol pyrophosphate synthases, inositol hexakisphosphate kinases (referred to as IP6Ks or Kcs1-like proteins) and diphosphoinositol pentakisphosphate kinases (known as PP-IP5Ks or Vip proteins) (Saiardi et al. 1999; Mulugu et al. 2007). These enzymes are primarily classified based on their catalytic specificity towards various positions on the inositol ring and their dual-domain protein architecture having a "rim-K" domain at the N-terminal and an ATP-grasp domain at the C-terminal (Lee et al. 2007; Mulugu et al. 2007).

Genes encoding VIH-type PP-InsP synthase could be identified in green algae and embryophytes (Desai et al. 2014; Laha et al. 2015). *Arabidopsis* VIH proteins catalyze the synthesis of the inositol pyrophosphate, $InsP_8$ and VIH-derived $InsP_8$ has been linked with diverse physiological processes such as plant defence and phosphate homeostasis (Laha et al. 2016; Jung et al. 2018; Dong et al. 2019; Zhu et al. 2019; Ried et al. 2021; Riemer et al. 2021) . It was further shown that $InsP_8$ binds to SPX1 protein and controls its interaction with the phosphate starvation response 1 (PHR1), a central regulator of phosphate starvation (Jung et al. 2018; Dong et al. 2019; Ried et al. 2021). It seems logical to conclude that higher levels of InsPx are co-related with the gain of function against different physiological processes.

Although the level of PP-InsPs seems to be important in asserting such function, it remains to be studied if the responsible kinases, especially plant VIH could interact physically with the components of the specific signalling system. One consequence could be local enrichment of PP-InsP species in the vicinity of their target proteins. There are multiple reports that suggests the employment of such gating of PP-InsP to its target proteins through physical interaction of the responsible PP-InsP synthase (Rao et al. 2014; Zhou et al. 2021; Laha et al. 2022; Bhandari et al. 2024). A comprehensive interaction studies for VIH protein is missing in plants that could provide new insights into how their signaling output is regulated.

Multiple VIH proteins were identified in hexaploid wheat with diphosphoinositol pentakisphosphate kinases (PP-InsP5K) like enzymatic activity (Shukla et al. 2021). Notably, when wheat VIH homolog (TaVIH2-3B) was expressed heterologously in *Arabidopsis*, they conferred tolerance to drought conditions (Shukla et al. 2021). Further, it was shown that VIH2 overexpressed lines show reprogramming of genes involved in cell-wall-related metabolic pathway genes. At the metabolome level, these transgenic lines showed high accumulation of cell-wall cementing polysaccharides such as arabinoxylan and arabinogalactan (Shukla et al. 2021). Although, the role of VIH was established in imparting drought tolerance in plants; it remains to be dissected if VIH could be involved at the protein level. Furthermore, it remains to be studied if VIH could function by protein-protein interactions.

Using a yeast two-hybrid (Y2H) screening system, we identified multiple interactors of TaVIH2-3B. Further, a detailed characterization was done for one of the interactors referred to as fasciclin-like arabinogalactan protein **(**FLA7) which is involved in the cell wall cementing process. Using biochemical experiments and a yeast genetic screen, we demonstrated that the presence of VIH-type PP-InsP synthase is required for FLA7 localization. This study expands our knowledge of the functioning of the plant VIHs towards new roles including cell-wall homeostasis.

Materials and methods

Wheat cDNA library construction and yeast two-hybrid screening

Total RNA extracted from the wheat seedlings was used to purify mRNA. mRNA was isolated by a plant mRNA isolation kit (Sigma). The mRNA concentration and purity were checked by nanodrop and 0.8% (w/v) agarose gel, then visualized by ethidium bromide staining under U.V light. Multiple batches of mRNA were pooled together to prepare the cDNA library, and single-strand cDNA was constructed as described in the materials and methods section. Next, the double-strand cDNA was prepared through long-distance PCR, and aliquots were analyzed in the 1.2% agarose/EtBr gel. Finally, the ds-cDNA was first purified using CHROMA SPIN+TE-400 columns. The wheat cDNA library was prepared by the co-transformation of the pGADT7-Rec vector provided in the kit and purified cDNA prepared (in the above section) in the Y187 yeast strain. The transformation mixture was

diluted (10^{-1} and 10^{-2}), and 100 µl of each dilution was plated on the SD-L agar plates to select independent clones, indicating the readiness of our library's complexity.

Gene expression analysis by quantitative real-time PCR

The hexaploid wheat cv. C-306 was used for this study. The grains of cv. C306 were stratified overnight in the dark at 4°C and then germinated for 4 days on Petri dishes lined with Whatman filter paper. The seven-day-old seedlings were subjected to drought mimic stress by exposing the roots of seedlings to 30% glycerol for six days along with Hoagland media. Control treatment was without any presence of glycerol in the media. Root and shoot tissue were collected post-treatment and Total RNA was extracted from the tissue from the three biological replicates. Expression in grains was studied as described earlier (Bhati et al., 2014). To quantify the gene expression in roots, quantitative real-time PCR (qRT-PCR) was performed using the QuantiTect SYBR Green RT-PCR Kit (Qiagen, Germany). The gene-specific primers capable of amplifying the genes mentioned in Table S1 were carefully designed using Oligocalc software. The cDNA dilutions to be used were optimized by running a semi-quantitative PCR for 22-25 cycles using Thermo Scientific™ DreamTaq™ Green PCR Master Mix (2X). The qRT-PCR reaction was set up in a 96-well plate by mixing the reaction components including 1X QuantiTect SYBR Green RT-PCR Master Mix, appropriate cDNA dilution, 900nM of forward and reverse primers and MQ to final volume of 10µl in each well and the plate was run in 7500 Fast Real-Time PCR System. 4-5 technical replicates for each set of primers and a minimum of 2 biological replicates were used to validate the experiment. ADP-ribosylation factor gene (*TaARF*) was used as an internal control in all the expression studies (Meena et al. 2024). The Ct values obtained after the run were normalized against the internal control and relative expression was quantified using $2^{-\Delta\Delta CT}$ method (Livak and Schmittgen 2001). The results for each sample are presented as the mean ± standard deviation (SD) from three replicates. Student's t-test was performed to assess the significance of differences between samples. A p-value of less than 0.05 (*) was considered statistically significant.P value < 0.05.

Co-immunoprecipitation of interacting proteins

For pull-down assays, respective yeast cultures were grown in SD media with appropriate amino acid dropouts. The primary culture was grown overnight at 30 ˚C until an OD_{600} of 1 was achieved. The secondary culture was incubated for 6 hours, cells were washed, and the lysate was prepared using glass beads in buffer (1% SDS, 100mM NaCl,100mM Tris-Cl,

1mM EDTA, 2% Triton and 1mM protease inhibitor (100X Halt protease inhibitor, Thermofisher, U.S.A.). The protein concentration in lysate was calculated at two dilutions. Equal amounts of each lysate were taken and incubated with 100% of Protein-G agarose beads and 2 ul of anti-c-MYC antibody for overnight at 4 ˚C. The lysate was subsequently washed three times with lysis buffer and centrifuged for 30 sec at 800 x g. 50 ul of loading dye was added to the washed beads and heated at 65 C for 10 min. After the SDS-PAGE run, the proteins were transferred to the PVDF membrane and processed. Blot was separated into two parts to detect TaVIH2 and TaFLA7 separately. Different primary antibodies were used for probing (mouse Anti-c-MYC and rabbit anti-HA with 1:2000 dilution). After washing the blots with TBST, they were treated with the secondary antibody (Goat Anti-Mouse IgG (H + L); and Goat Anti-Rabbit IgG (H + L) with 1:5000 dilution. After subsequent washing with TBST, the blot was developed by using BIO-RAD clarity western ECL Substrate.

Localization studies

TaFLA7 was cloned in pGADT7 vector at *EcoR*1 and *BamH*1 sites for the localization experiments. TaVIH2 cDNA was cloned in the pGBKT7 vector using Sma1 and Not1 restriction sites. The constructs were transformed in the Y2H Gold yeast strain and selected on SD-Leu or SD-Trp plates. Yeast spheroplasts were prepared for localization as described earlier (Severance et al., 2004). Mouse monoclonal Anti-HA (H.A.:FLA7-pGADT7) : or rabbit Anti-c-Myc (cMYC: VIH2-pGBKT7) primary antibody (Invitrogen, USA) was used for the respective preparations at a ratio of 1:200 followed by 5 washing with blocking buffer. Yeast cells were incubated with Goat Anti-Mouse IgG (H+L) Alexa Flour Plus 488 or Goat Anti-Rabbit IgG (H+L) Alexa Flour Plus 647 (Invitrogen, USA) at a ratio of 1:500 for 4hr at room temperature. Cells were washed with blocking buffer and mounted with Fluor mount (Sigma, USA). Representative fluorescent images were taken using LEICA DM600CS using a 64X oil objective.

Luciferase Assay

Coding sequences (CDS) of TaVIH2 and TaFLA7 was amplified using forward primers containing *BamH*I and reverse primers containing *EcoR*I, ensuring that the open reading frame (ORF) remained intact. The amplified products were then cloned into pCAMBIA1300-NLuc and pCAMBIA1300-CLuc vectors. The recombinant plasmids were initially transformed into *E. coli* DH5α cells for propagation and were confirmed by sequencing. Subsequently, the verified plasmids were transformed into the *Agrobacterium tumefaciens*

GV3101 strain. Positive clones of GV3101 containing the recombinant plasmids were selected and cultured overnight with appropriate antibiotics. The cells were pelleted and resuspended in freshly prepared induction media containing 10 mM $MgCl_2$, 10 mM MES (pH 5.7), and 150 µM acetosyringone. The optical density (OD) of each culture was adjusted to 0.5, and 1 mL of the Nluc-expressing cells was mixed with 1 mL of the Cluc-expressing cells. The mixture was incubated at 28°C without shaking for 5–6 hours before agroinfiltration into tobacco leaves (10 µL per spot, with three spots per leaf). The infiltrated plants were maintained in a humidity chamber, kept in the dark for 12 hours, and then exposed to light for 24 hours. Finally, the leaves were harvested and chemiluminescence was detected, with an exposure time set at 20 seconds.

Extraction of Inositol Pyrophosphates

S. cerevisiae cultures were grown at 30°C in Synthetic Complete Dextrose (SCD) media until they reached exponential growth, with an A_{600} between 0.6 and 0.8. Cells equivalent to 10 A_{600} units were collected by centrifugation. After washing with ice-cold water, the cells were resuspended in 500 µL of 1 M perchloric acid. The samples were quickly frozen using liquid nitrogen and stored at −80°C. Upon thawing, the samples were briefly vortexed, and cell debris was removed by centrifugation at 16,200 g for 5 minutes at 4°C. The supernatants containing acid-extracted inositol polyphosphates were then purified using titanium dioxide beads (GL Sciences 5020–75000), following the method described by (Wilson and Saiardi 2017). Specifically, the supernatants were combined with 5 mg of TiO2 beads per sample, pre-washed with water and 1 M perchloric acid, followed by incubation on a nutator at 4°C for 20 minutes. The beads with bound inositol polyphosphates were collected by centrifugation at 5,000 g for 1 minute at 4°C, followed by two washes with 1 M perchloric acid. To elute the inositol polyphosphates, the beads were resuspended twice in 250 µL of 3% ammonium hydroxide, rotated for 5 minutes at 4°C, and then centrifuged at 5,000 g for 1 minute. The combined eluates (totalling 500 µL per sample) were dried using a vacuum centrifuge (Eppendorf SpeedVac) at room temp. for approximately 5 hours. The dried samples were reconstituted in 20 µL of water for capillary electrophoresis electrospray ionization mass spectrometry (CE-MS) analysis.

Capillary electrophoresis–mass spectrometry (CE-MS) analysis

The CE-MS analyses were conducted as described in (Qiu et al. 2020, 2023; Saiardi et al. 2021). An Agilent CE-QQQ system was used for the analysis, which featured an Agilent

7100 capillary electrophoresis unit, an Agilent 6495C Triple Quadrupole mass spectrometer, and an Agilent Jet Stream electrospray ionization source, all connected via an Agilent CE-ESI-MS interface. The sheath liquid, a 50:50 combination of isopropanol and water, was given at a steady flow rate of 10 µL/min using an isocratic Agilent 1200 LC pump and a splitter to ensure exact flow. A 100 cm long fused silica capillary with an internal diameter of 50 µm and an outside diameter of 365 µm was employed to separate the samples.

The background electrolyte (BGE) contained 40 mM ammonium acetate that had been adjusted to pH 9.08 with ammonium hydroxide. Before each sample analysis, the capillary was flushed with BGE for 400 seconds. Samples were delivered into the system by applying a pressure of 100 mbar for 15 seconds, resulting in an injection volume of around 30 nL. The MS source settings included a gas temperature of 150˚C, flow rate of 11 L/min, nebulizer pressure of 8 psi, and sheath gas temperature of 175˚C. The capillary voltage was set to -2000V, with a nozzle voltage of 2000V. Furthermore, the negative high-pressure radio frequency (RF) and negative low-pressure RF were kept at 70 and 40 volts, respectively. The multiple reaction monitoring (MRM) parameters were set up as shown in Table 1.

The internal standard (IS) stock solution was created using the method described in (Qiu et al. 2020; Saiardi et al. 2021). Which was then added to the samples to help with isomer assignment and quantification of InsPs and PP-InsPs. 5 µL of IS was added to 5 µL of sample and carefully mixed. IPs were quantified by adding known amounts of the matching heavy isotopic references to the samples. After spiking, the final concentrations in the samples were as follows: 4 µM [$^{13}C_6$] 2-OH $InsP_5$, 20 µM [$^{13}C_6$] $InsP_6$, 1 µM [$^{13}C_6$] 5- $InsP_7$, 1 µM [$^{13}C_6$] 1-$InsP_7$, and 1 µM [$^{13}C_6$] 1,5- $InsP_8$. Dorothea Fiedler provided the [13C6] inositol STD (Harmel et al. 2019).

Results

VIH proteins contain variable IDR regions

Studies in the yeast and mammalian systems have shown that different inositol pyrophosphate kinase function is based on their protein interaction networks (Gokhale 2013; Rao et al. 2014; Wright and Dyson 2015; Rogers et al. 2021a). The human PPIP5K (HsPPIP5K) interaction studies show the typical dual domains involvement and requirement of the C-terminal intrinsically disordered region (IDR) for interaction (Machkalyan et al. 2016). This HsPPIP5K contains a large C-terminal IDR region (~250-550 aa), a missing

characteristic for most plant VIHs (Figure 1& Figure S1). The IDR region was checked in the plant VIH proteins. Our analysis indicated that plant VIH proteins have a variable and lower percentage of IDR representation. The plants VIH show 12-22 % of IDR region (Table 2). Interestingly, wheat TaVIH possesses a higher IDR % when compared to the *Arabidopsis* (Figure 1).

To get insights into the direct and indirect interactions, we performed a String analysis of VIH proteins. Human PPIP5K and yeast (VIP1) analysis resulted in the protein-protein network analysis with nodes pointing towards the PHO-mediated interactors for the VIP and involvement of HsPPIP5K in other biochemical activities (Figure 2). A similar analysis of wheat VIH2-3B protein shows multifunctional globular proteins such as actin as probable interactors. The presence of IDR in the wheat VIH2 and the preliminary String analysis led us to explore its interacting partners.

Screening of TaVIH2 interacting partners

To get molecular insights into the role of TaVIH2 proteins in stress tolerance, we used yeast two-hybrid (Y2H) cDNA library screen to identify its possible interacting partners. Protein expression of bait (VIH2) in the yeast cells was confirmed by immunoblot analysis (Supplementary Figure S2A). Two pooled wheat cDNA libraries were prepared for Y2H studies. The resulting smear between 300 bp to 5 kb confirmed the good quality of ds-cDNA (Supplementary Figure S2B). Y2H was performed using TaVIH2-3B as a bait and this resulted in the identification of 89 putative yeast colonies with a mating efficiency of 3.8 %. Subsequent screening of the colonies led to the identification of ~52 putative interactors (Supplementary Figure S2C&D). Amplicons were sequenced and clones appearing more than twice were considered for further studies (Supplementary Figure S3). The analysis led to the shortlisting of ten strong potential interactors with high occurrence in the screening (Table 3). Amongst these interactors, most of the genes encode for cell-wall-related function, including fasciclin-like arabinogalactan protein (FLA), glycosyl-transferases, and glycine-rich structural proteins. The most frequently (nine times) interacting clone was identified as FLA7 (*TraesCS2D02G172900*) protein, and further detailed characterization was performed with this protein. Our analysis indicated that TaFLA7 encodes a 367 aa protein containing FAS-like arabinogalactan protein and the presence of a typical transmembrane domain (TMD) with glycophosphatidyl-inositol (GPI) domain along with hydrophobic domains (Figure S4). Additionally, the protein hydropathy plot identified a hydrophobic region near the GPI region at the C-terminal.

Wheat VIH2 interacts with fasciclin-like arabinogalactan protein (FLA)

To further confirm this interaction, full-length coding sequence of *TaFLA7* (1.2 kb) was cloned (TaFLA7:AD+TaVIH2:BD) and co-transformed along with TaVIH2 in the yeast strain. The yeast co-transformed with TaFLA7 and TaVIH2 showed strong reporter activity (Figure 3A). To further confirm this interaction, yeast colonies were grown on -His/-Leu/-Trp (Auerobasidin) media (Figure 3B) and the protein extracts were subjected to *in vivo* pull□down assay. For this, first we checked the expression of HA-tagged FLA7 and c-MYC-tagged TaVIH2 in the Y2H Gold yeast strain. Western analysis for both proteins (TaFLA7 ~55 kDa) indicated optimal expression in the cells (Figure 3B). Furthermore, only the TaVIH2 was detected in the yeast strain lacking TaFLA7 (Figure 3B) compared to the control (Figure 3B). However, in the pull-down analysis of TaFLA7 and TaVIH2 co-transformed cells, both the TaFLA7 and TaVIH2 proteins were detected (Figure 3B; Lane 4). These findings imply that TaVIH2 and TaFLA7 show protein-protein interaction. To further validate this interaction, we performed split luciferase complementation assayusing tobacco leaf (*Nicotiana benthamiana*) with the fused protein NLuc-TaFLA7)/CLuc-TaVIH2. Luciferase complementation imaging (LCI) pair reconstituted luciferase activity in regions where both the fused proteins were expressed when compared to controls (Figure 4A). RLU measurement suggested an increase of 7-8 folds of the luminescence activity compared to the controls (Figure 4B). Overall, these results confirmed that TaVIH2 nteract with cell-wall cementing proteins.

VIH2 facilitates the localization of FLA7

Next, we studied the localization of the FLA7 protein in yeast cells. Confocal imaging of yeast cells expressing TaFLA7:GFP suggests its presence on the plasma membrane (Figure 5A). Since the wheat FLA7-VIH2 interact and FLA7 is localized to the membrane, we wonder whether VIH2-3B contributes to the localization of FLA7. Previously, we reported that *TaVIH2-3B* overexpressing lines enhanced the expression of genes involved in cell wall biosynthesis (Shukla et al. 2021). TaVIH2-3B was shown to utilize IP_7 as a substrate likewise to yeast VIP1. Therefore, we tested the localization of FLA7 in different yeast backgrounds. As expected, in the WT yeast, FLA7 was localized on the plasma membrane, but surprisingly this localisation was affected in the VIP1-deficient yeast cells (Figure 5B). This suggested that localization of the FLA7 is dependent on VIP1 activity. Next, we complemented the yeast *vip1*Δ mutant and checked for the FLA7 localization. Interestingly,

the presence of TaVIH2-3B restores the localisation of TaFL6 to the plasma membrane in the the yeast *vip1*Δ strain.

Additionally, we have also profiled the cellular pools of $InsP_6$, 5-$InsP_7$, 1-$InsP_7$, and 1,5-$InsP_8$ with capillary electrophoresis electrospray ionization mass spectrometry (CE-ESI-MS), as described in (Qiu et al. 2020, 2023; Saiardi et al. 2021; Liu et al. 2023; Eisenbeis et al. 2023). This method allows us to investigate the cellular levels of different InsP and PP-InsP species in the yeast transformants. To account for any differences in sample recovery during extraction and TiO_2 bead affinity enrichment, the levels of 5-$InsP_7$, 1-$InsP_7$, and 1,5-$InsP_8$ were normalized to $InsP_6$ levels (Figure. 6). The observed changes in the 1,5-$InsP_8$ levels (Figure. 6) between the WT, *vip1*Δ mutant and *vip1*Δ::TaVIH2-3B complimented extracts confirmed that TaVIH2 is a functional $InsP_8$ synthase in yeast and it is likely that the localization of TaFLA7 is dependent of the TaVIH2-derived $InsP_8$. Collectively, our results indicate that TaVIH2-3B interacts with the FLA7 protein and could facilitate its localization to the plasma membrane. Moreover, the differences in 1,5-$InsP_8$ levels witnessed among the WT, *vip1*Δ mutant, and *vip1*Δ mutant complemented with TaVIH2-3B suggest that the appropriate positioning of TaFLA7 is associated with the activity of the PP-InsP5K enzyme.

FLA7 is differentially expressed in wheat tissue and is induced by drought condition

The FLA proteins are known to respond to different stress conditions and are involved in plant growth and development (Zang et al. 2015; Cagnola et al. 2018; Wu et al. 2020; Ma et al. 2022; Yao et al. 2023). These observations suggest that VIH2 and its interacting partners could participate in similar pathways. To further characterize the wheat *FLA7*, we studied its expression in different tissues and under different stress conditions. Our analysis suggested that TaFLA7 was expressed in the grain at the Z71 stage (watery ripe with the start of grain filling) and in the spike at Z65 (50% of the spikes had yellow anthers) of wheat development (Figure 7A). Expression analysis of *TaFLA7* in different wheat grain tissue using the eFP wheat browser revealed its high expression in embryo and aleurone layers of the grain (Figure 7B). The eFP wheat browser analysis indicates the high expression of FLA7 in grains, shoot axis and spikelet (Figure 7B&C; Figure S5, Figure S6). In grains the expression was higher in the outer and inner pericarp region. Our qRT-PCR during garin development suggest increasing expression of TaFLA7 mRNA with its maturation with highest expression at 28 days after the anthesis DAA (Figure 7D). Based on the previous in-silico data the transcript expression of *TaFLA7* showed significant upregulation in the shoot tissue when subjected to drought stress after 1 hr and 6 hrs (Figure 7E). Our quantitative RT-PCR results

also confirmed the significant upregulation of TaFLA7 in the shoot or root tissue subjected to drought stress (Figure 7F). Altogether the expression data of the *TaFLA7* show transcriptional changes during desiccation, a prerequisite step in grain maturation.

Discussion

Protein-protein interaction networks provide valuable insights into biological processes and complex metabolic functions within living cells. The Y2H system leverages eukaryotic transcriptional activators with distinct functional domains for DNA-binding and transactivation, making it a powerful and rapid approach to discovering new protein interactions (He et al. 2019). In this study, a high-quality yeast two-hybrid (Y2H) library using RNA extracted from wheat seedlings was constructed. Our work identified several interactors of TaVIH2 proteins, which serve as promising entry points for further exploration of their regulatory network in the developmental process. Recently, it was demonstrated that the *Triticum aestivum* (hexaploid wheat) genome encodes functional PPIP5K isoforms, identified as TaVIH2-3B (Shukla et al. 2021). Moreover, the heterologous expression of wheat TaVIH2-3B in *Arabidopsis* imparts drought tolerance. These *Arabidopsis* transgenic lines expressing TaVIH2 also exhibit a reprogramming of gene expression involved in cell-wall metabolism and stress response pathways (Shukla et al. 2021). In particular differential expression of genes linked to ABA biosynthesis, cell wall maintenance, and cytochrome P-450 monooxygenases were highly upregulated. Although the level of InsPs seems to be important in imparting such a function, it remains to be studied if plant PP-InsP synthase, such as VIH at the protein level, could be involved directly.

Multi-protein interactions were more accessible by IDRs, which helped them connect with other proteins in the cell. Abelson (Abl), a protein non-receptor tyrosine kinase, has an IDR domain (around 900 amino acids) that has been implicated in a variety of tasks in *Drosophila*, including the regulation of cell shape and cytoskeleton development (Rogers et al. 2021b). Similarly, the human PPIP5K domains' association with proteins involved in actin cytoskeleton structure and phosphatidylinositol biosynthesis was attributed to the IDR's existence (Machkalyan et al. 2016). The interaction studies were pursued using human PPIP5K (HsPPIP5K) (Machkalyan et al. 2016). Human PPIP5K, besides containing the typical dual-domain, also possesses a C-terminal IDR (Machkalyan et al. 2016). This IDR in HsPPIP5K spans a large portion (~250-550 amino acids), a feature that is not very common

in most plant VIHs (Figure 1). IDRs assist in their interaction with multiple proteins to facilitate their cellular activities (Ward et al. 2004).

Although VIH proteins have been identified in several plants (Laha et al. 2015; Zhu et al. 2019), including wheat (Shukla et al. 2021), the IDR domains are relatively smaller, ranging from approximately 33-56 amino acids, and their functional roles remain to be elucidated. Our network analysis using the String database can provide clues for the regulatory network of the VIH proteins (Figure 2). Human PPIP5K and yeast (VIP1) analysis resulted in the protein-protein network analysis with nodes pointing towards the PHO-mediated interactors for the VIP and involvement of HsPPIP5K in other biochemical activities (Figure 2). A similar analysis of wheat VIH shows a network with cytoskeletal actin as a probable interactor. Actin is involved in forming microfilaments in the cytoskeleton and can modulate the cellular shape (Pollard and Cooper 2009). This study identified multiple interactors of VIH2, yet most of them are speculated to be involved in cell wall maintenance. The speculative parallels of VIP1 in yeast and VIH encouraged us to postulate that plant VIH is likely involved in cell wall cementing and homeostasis. The conserved role of VIH was demonstrated in the important cellular function of Pi-homeostasis (Dong et al. 2019; Zhu et al. 2019; Riemer et al. 2021). Under nutrient-limiting conditions, VIP1 and its ortholog in *Schizosaccharomyces* pombe (Asp1) kinase were shown to control physiological changes such as dimorphic switch, cell-to-cell, cell-substrate adhesion and unipolar budding (Pöhlmann and Fleig 2010; Pöhlmann et al. 2014). The ability of TaVIH2 to facilitate the localization of TaFLA7 (Figure 5) provides new insight into the functioning of VIH proteins. The involvement of these proteins in this process points towards their ability to control the cellular boundaries and shape (Figure 8). Such phenotypic changes, including the formation of pseudo-hyphal filaments in yeast (Norman et al. 2018), help sustain themselves under stress conditions, yet their similar involvement in plants needs more investigation. Previous biochemical investigations of TaVIH2-3B overexpressing lines in *Arabidopsis* indicated changes in cell wall cementing metabolites such as cellulose, arabino-xylan, and arabino-galactan (Shukla et al. 2021). Furthermore, RNAseq analysis of the Col-0 and TaVIH2 overexpressing lines suggested high expression of genes involved in cell wall biosynthesis (Shukla et al. 2021). Together with these results, our findings suggest that VIH2 can regulate the composition of cell wall cementing pathways by localizing the involved proteins to their correct positions. The intriguing role of VIH protein overexpression in modulating cell wall composition requires further investigation. Specifically, the *in-vivo* levels of $InsP_7$/$InsP_8$ (Figure 6) suggest that TaVIH2-3B possess PP-IP5K enzymatic activity. Therefore, either the

synthesis of $InsP_8$ or the presence of TaVIH2-3B protein in the yeast cell directly influences the correct localization of the TaFLA7 to the plasma membrane. Furthermore, it is crucial to investigate how this localization occurs and to identify which region of TaFLA7 interacts with TaVIH2-3B and understanding the role in such interaction may also be critical for future study. In the aftermath of the current study, it will be interesting to check if $InsP_7$/$InsP_8$ could modulate the protein-protein interactions of transcription factors that are primarily involved in water-deficient stress conditions. This remains to be investigated and could offer new mechanistic insights into drought tolerance. Studies using *Arabidopsis* have deciphered multiple roles of VIHs in different biological processes. However, such efforts should be expanded to crop plants such as wheat for translational research.

Acknowledgements

The authors thank the Executive Director for the facilities and support. This study was supported by the Department of Biotechnology, Basic Plant Biology Grant to AKP [BT/PR12432/BPA/118/35/2014]. Part of this work was also supported by the NABI-CORE grant to A.K.P. and by the Deutsche Forschungsgemeinschaft (DFG) under Germany's Excellence Strategy CIBSS, EXC-2189, Project ID 390939984 to H.J. DBT-eLibrary Consortium (DeLCON) is acknowledged for providing timely support and access to e-resources for this work. A.S. acknowledges Centre For Integrative Biological Signalling Studies for PostDoctral Fellowship. D. L. acknowledges the Department of Biotechnology (DBT) for HGK-Innovative Young Biotechnologist Award (BT/13/IYBA/2020/04).

Declarations

Conflict of interest

The authors declare that they have no known competing financial interests or personal relationships that could have appeared to influence the work reported in this manuscript.

Authors contribution

AKP and AS conceived the project. AS, AKP and RT designed the experiments. AS, RT, RG and KA performed the experiments. AKP, AS, DL and HJ wrote and revised the draft manuscript. All the authors commented on the manuscript and agreed to the submission of the manuscript.

Data Availability

No datasets were generated or analysed during the current study.

Figures for the legends:

Figure 1: *In-silico* calculation of the Intrinsic Disorder Regions (IDR) of VIH and PPIP5K proteins. IDR was calculated based on the xxx along with the percentage region score of the mentioned proteins.

Figure 2: Protein association networks were identified for each of the human (PPIP5K1), yeast (VIP1) and wheat (VIH; Traes_3B_3567813F3.1). The network analysis for each of the proteins was performed using STRING and was represented as the coloured lines with the description as given in the figure.

Figure 3: Interaction of TaVIH2-3B with TaFLA7 as identified during Y2H screening. (A) Y2H assay using full-length TaFLA7 and VIH as represented by GAL plates containing -L-T and without GAL plates containing -HLT. (B) Pull-down assay and Western analysis of the wheat FLA7 in the yeast strains.

Figure 4: Luciferase reporter assay to characterization of TaFLA7 interaction with FLA7. (A) Luciferase assay of TaFLA7 with VIH2 using tobacco leaves. **(B)** RLU measurement for the strength of interaction. The values shown are the mean ± SE; n = 4. Student's *t* test was performed (*$p < 0.001$).

Figure 5: The localization of TaFLA7 and its dependency on the VIH2 activity. (A) Protein structure arrangements of TaFLA7 protein and localization in yeast cells. (B) In situ localization of the TaFLA7 to the membrane in the yeast vip1 mutant transformed with TaVIH2-3B. Localization of FLA7 using HAtagged-TaFLA7 in different yeast strains. Fluorescence was measured using a Zeiss fluorescence microscope (Axio Imager Z2) with an Axiocam MRm camera at 63X. Representative images are shown and similar observations were noted for 3-4 independent transformed colonies of yeast.

Figure 6: Quantification of inositol pyrophosphate levels using CE-ESI-MS. The inositol pyrophosphate levels in extracts of the WT + pYES2 , *vip1*Δ + pYES2, and *vip1*Δ + TaVIH2-3B strains that were transformed with TaFLA7 are displayed for 1,5-$InsP_8$, 5-$InsP_7$, and 1-$InsP_7$, normalized to the levels of $InsP_6$. The values shown are the mean ± SE; n = 3. Student's *t* test was performed (*$p < 0.001$).

Figure 7. Expression characterization of TaFLA7 in wheat tissue. (A) Relative gene expression level during plant development (at Zadosky scale; Exvip database; https://dubcovskylab.ucdavis.edu/expression_data/). (B) Expression (TPM: transcript per million) of the FLA7 in developed grains of wheat. Heat map indicates Log_2ratio. (C)

Expression (TPM: transcript per million) of TaFLA6 in grain layers; endosperm, inner pericarp and outer pericarp. (D) Expression of TaFLA7 during grain development. stages of embryo development. (E) The expression profiles of the TaFLA7 in roots and shoot tissue of wheat seedlings collected at 6 days under drought stress. (F) qRT-PCR analysis of TaFLA7 after drought mimic condition (30% glycerol) in shoots and roots. CR: control roots; RT: Root treatment; CS: Control shoot: and ST: shoot treatment.

Figure 8: Schematic representation drawing parallels for the possible function of VIH proteins in multiple cellular processes. In yeast, VIP proteins and their products were shown to be involved in the cell boundary rearrangements which include regulation of microtubule rearrangement and filamentous growth of the fungi under nutrient-limiting conditions (Pöhlmann and Fleig 2010; Pöhlmann et al. 2014). Plant VIHs are known to be involved in phosphate (Pi) homeostasis and plant defence (Laha et al. 2015; Dong et al. 2019; Riemer et al. 2021). Recently, the role of plant VIH in cell wall-related rearrangements has been established (Shukla et al. 2021). The participation of genes encoding VIP1/VIH proteins in cell wall rearrangement in both yeast and plants could reflect the conserved function of the proteins across species (Pöhlmann et al. 2014; Shukla et al. 2021).

Table 1: MS parameters for MRM transitions

Molecular name	Precursor Ion	Product Ion	Collision Energy (V)	Cell Accelerator Voltage
$[^{13}C_6]$ $InsP_5$	292	504.9	9	3
$InsP_5$	289	498.9	9	3
$[^{13}C_6]$ $InsP_6$	331.9	79.1	53	4
$InsP_6$	328.9	79.1	53	4
$[^{13}C_6]$ $InsP_7$	371.9	322.9	9	3
$[^{18}O_2]$ 4-$InsP_7$	370.9	319.9	9	3
$InsP_7$	368.9	319.9	9	3
1,5$[^{13}C_6]$ $InsP_8$	411.9	362.8	9	1
1,5$InsP_8$	408.9	359.8	9	1

Polarity: Negative, Dwell: 80, Fragmentor (V): 166

Table 2: Intrinsic disorder region (IDR) percentage, length and position in the human and plant encoded PPIP5K-like proteins. The efficient disorder prediction was made using ESpritz (ver1.3).

Name	% Disorder	Length of largest segment	Position	Position in AA	Total AA
HsIP6K1	29.58	167	After 8th	1107 to 1274	1433
HsIP6K2	29.92	155	After 9th	873 to 1028	1243
AtVIH1	13.34	65	After 4th	792 to 857	1049
AtVIH2	12.40	69	After 4th	797 to 866	1056
OsVIH1	16.47	81	After 3rd	786 to 867	1043
OsVIH2	10.54	30	After 3rd	648 to 678	758
TaVIH2-3B	12.93	37	After 5th	815 to 837	1036
TaVIH1-4D	13.65	56	After 5th	797 to 853	1047

Table 3: Interacting partners of wheat VIH2 proteins. The tables indicate the gene IDs with their annotated function based on homology. The numbers indicate the frequency of the occurrence of the clone as an interacting partner from the library.

S.No	Gene Function	Known functional in Planta	New TRIAE_ ID	Number of Occurrences
1.	**Fasciclin-like protein FLA7**	Cell wall biosynthesis, stress response,	TraesCS2D02G172900.1	9
2.	**Glycosyl-transferases (GT1)**	Cell wall biosynthesis, stress response, cell wall cementing, transfer sugar moieties	TraesCS6B02G339100.1	6
3.	**Xylan arabinosyl transferase (Xat1)**	Cell wall biosynthesis, stress response, cell wall cementing	TraesCS6A02G309400.1	5
4.	**Glycine-rich cell wall structural protein-like**	Cell wall biosynthesis, stress response	TraesCS2B02G541900	5
5.	**NADH-ubiquinone reductase complex 1 MLRQ subunit;**	Uncharacterized protein	TraesCS7A02G238600	3
6.	**Hypothetical protein TRIUR3_12806**	Auxin efflux transporter that acts as a negative regulator of light signalling to promote hypocotyl elongation	TraesCS4A02G016700	3
7.	**ABC**	Metal transporter involved	TraesCS5A02G392600	4

	transporter B family member	in the sequestration of aluminium into vacuoles		
8.	**Short-chain dehydrogenase reductase**	Glucose signalling and abscisic acid biosynthesis and functions	TraesCS2B02G116700	3
9.	***Ethylene-responsive element binding protein 1 (EREB1)***	Increases tolerance to abiotic stress	TraesCS7B02G062200	4
10	**W.W. domain-binding protein (containing PPG PPP motif)**	Modules mediate protein-protein interactions by recognizing proline-rich peptide motifs and phosphorylated serine/threonine-proline sites.	TraesCS7B02G062200	3

Reference:

Azevedo C, Burton A, Ruiz-Mateos E, et al (2009) Inositol pyrophosphate mediated pyrophosphorylation of AP3B1 regulates HIV-1 Gag release. Proc Natl Acad Sci 106:21161–21166. https://doi.org/10.1073/pnas.0909176106

Bhandari R, Hamid A, Ladke JS, et al (2024) Interaction with IP6K1 supports pyrophosphorylation of substrate proteins by the inositol pyrophosphate 5-InsP7. Biosci Rep BSR20240792. https://doi.org/10.1042/BSR20240792

Bhati K, Aggarwal S, Sharma S, et al (2014) Differential expression of structural genes for the late phase of phytic acid biosynthesis in developing seeds of wheat (*Triticum aestivum* L.). Plant Science 224: 74-85

Cagnola JI, Dumont de Chassart GJ, Ibarra SE, et al (2018) Reduced expression of selected FASCICLIN-LIKE ARABINOGALACTAN PROTEIN genes associates with the abortion of kernels in field crops of Zea mays (maize) and of Arabidopsis seeds. Plant Cell Environ 41:661–674. https://doi.org/https://doi.org/10.1111/pce.13136

Chabert V, Kim G-D, Qiu D, et al (2023) Inositol pyrophosphate dynamics reveals control of the yeast phosphate starvation program through 1,5-IP(8) and the SPX domain of Pho81. Elife 12:. https://doi.org/10.7554/eLife.87956

Desai M, Rangarajan P, Donahue JL, et al (2014) Two inositol hexakisphosphate kinases drive inositol pyrophosphate synthesis in plants. Plant J 80:642–653. https://doi.org/10.1111/tpj.12669

Dong J, Ma G, Sui L, et al (2019) Inositol Pyrophosphate InsP8 Acts as an Intracellular Phosphate Signal in Arabidopsis. Mol Plant 12:1463–1473. https://doi.org/10.1016/j.molp.2019.08.002

Eisenbeis VB, Qiu D, Gorka O, et al (2023) β-lapachone regulates mammalian inositol pyrophosphate levels in an NQO1- and oxygen-dependent manner. Proc Natl Acad Sci 120:e2306868120. https://doi.org/10.1073/pnas.2306868120

Fridy PC, Otto JC, Dollins DE, York JD (2007) Cloning and Characterization of Two Human VIP1-like Inositol Hexakisphosphate and Diphosphoinositol Pentakisphosphate Kinases. J Biol Chem 282:30754–30762. https://doi.org/10.1074/jbc.m704656200

Gokhale NA (2013) Membrane phosphoinositides and protein–membrane interactions. Amino Acids 45:751–754. https://doi.org/10.1007/s00726-013-1512-2

Harmel RK, Puschmann R, Nguyen Trung M, et al (2019) Harnessing (13)C-labeled myo-inositol to interrogate inositol phosphate messengers by NMR. Chem Sci 10:5267–5274. https://doi.org/10.1039/c9sc00151d

He Y, Wu L, Liu X, et al (2019) Yeast two-hybrid screening for proteins that interact with PFT in wheat. Sci Rep 9:15521. https://doi.org/10.1038/s41598-019-52030-x

Jung J-Y, Ried MK, Hothorn M, Poirier Y (2018) Control of plant phosphate homeostasis by inositol pyrophosphates and the SPX domain. Curr Opin Biotechnol 49:156–162. https://doi.org/https://doi.org/10.1016/j.copbio.2017.08.012

Laha D, Johnen P, Azevedo C, et al (2015) VIH2 Regulates the Synthesis of Inositol Pyrophosphate InsP8 and Jasmonate-Dependent Defenses in Arabidopsis. Plant Cell 27:1082–1097. https://doi.org/10.1105/tpc.114.135160

Laha D, Parvin N, Dynowski M, et al (2016) Inositol Polyphosphate Binding Specificity of the Jasmonate Receptor Complex . Plant Physiol 171:2364–2370. https://doi.org/10.1104/pp.16.00694

Laha NP, Giehl RFH, Riemer E, et al (2022) INOSITOL (1,3,4) TRIPHOSPHATE 5/6 KINASE1-dependent inositol polyphosphates regulate auxin responses in Arabidopsis. Plant Physiol 190:2722–2738. https://doi.org/10.1093/plphys/kiac425

Lee Y-S, Mulugu S, York JD, O'Shea EK (2007) Regulation of a cyclin-CDK-CDK inhibitor complex by inositol pyrophosphates. Science 316:109–112. https://doi.org/10.1126/science.1139080

Liu G, Riemer E, Schneider R, et al (2023) The phytase RipBL1 enables the assignment of a specific inositol phosphate isomer as a structural component of human kidney stones. RSC Chem Biol 4:300–309. https://doi.org/10.1039/d2cb00235c

Livak KJ, Schmittgen TD (2001) Analysis of Relative Gene Expression Data Using Real-Time Quantitative PCR and the 2−ΔΔCT Method. Methods 25:402–408. https://doi.org/10.1006/meth.2001.1262

Ma Y, MacMillan CP, de Vries L, et al (2022) FLA11 and FLA12 glycoproteins fine-tune stem secondary wall properties in response to mechanical stresses. New Phytol 233:1750–1767. https://doi.org/10.1111/nph.17898

Machkalyan G, Trieu P, Pétrin D, et al (2016) PPIP5K1 interacts with the exocyst complex through a C-terminal intrinsically disordered domain and regulates cell motility. Cell Signal 28:. https://doi.org/10.1016/j.cellsig.2016.02.002

Meena V, Kaur G, Joon R, et al (2024) Transcriptome and biochemical analysis in hexaploid wheat with contrasting tolerance to iron deficiency pinpoints multi-layered molecular process. Plant Physiol Biochem 207:108336. https://doi.org/https://doi.org/10.1016/j.plaphy.2024.108336

Mulugu S, Bai W, Fridy P, et al (2007) A Conserved Family of Enzymes That Phosphorylate Inositol Hexakisphosphate. Science 316:106–109. https://doi.org/10.1126/science.1139099

Norman KL, Shively CA, De La Rocha AJ, et al (2018) Inositol polyphosphates regulate and predict yeast pseudohyphal growth phenotypes. PLoS Genet 14:e1007493–e1007493. https://doi.org/10.1371/journal.pgen.1007493

Pipercevic J, Kohl B, Gerasimaite R, et al (2023) Inositol pyrophosphates activate the vacuolar transport chaperone complex in yeast by disrupting a homotypic SPX domain interaction. Nat Commun 14:2645. https://doi.org/10.1038/s41467-023-38315-w

Pöhlmann J, Fleig U (2010) Asp1, a Conserved 1/3 Inositol Polyphosphate Kinase, Regulates the Dimorphic Switch in Schizosaccharomyces pombe. Mol Cell Biol 30:4535. https://doi.org/10.1128/MCB.00472-10

Pöhlmann J, Risse C, Seidel C, et al (2014) The Vip1 inositol polyphosphate kinase family regulates polarized growth and modulates the microtubule cytoskeleton in fungi. PLoS Genet 10:e1004586–e1004586. https://doi.org/10.1371/journal.pgen.1004586

Pollard TD, Cooper JA (2009) Actin, a central player in cell shape and movement. Science 326:1208–1212. https://doi.org/10.1126/science.1175862

Qiu D, Gu C, Liu G, et al (2023) Capillary electrophoresis mass spectrometry identifies new isomers of inositol pyrophosphates in mammalian tissues. Chem Sci 14:658–667. https://doi.org/10.1039/d2sc05147h

Qiu D, Wilson MS, Eisenbeis VB, et al (2020) Analysis of inositol phosphate metabolism by capillary electrophoresis electrospray ionization mass spectrometry. Nat Commun 11:6035. https://doi.org/10.1038/s41467-020-19928-x

Rao F, Cha J, Xu J, et al (2014) Inositol pyrophosphates mediate the DNA-PK/ATM-p53 cell death pathway by regulating CK2 phosphorylation of Tti1/Tel2. Mol Cell 54:119–132. https://doi.org/10.1016/j.molcel.2014.02.020

Ried MK, Wild R, Zhu J, et al (2021) Inositol pyrophosphates promote the interaction of SPX domains with the coiled-coil motif of PHR transcription factors to regulate plant phosphate homeostasis. Nat Commun 12:384. https://doi.org/10.1038/s41467-020-20681-4

Riemer E, Qiu D, Laha D, et al (2021) ITPK1 is an InsP6/ADP phosphotransferase that controls phosphate signaling in Arabidopsis. Mol Plant 14:1864–1880. https://doi.org/https://doi.org/10.1016/j.molp.2021.07.011

Rogers EM, Allred SC, Peifer M (2021a) Abelson kinase's intrinsically disordered region plays essential roles in protein function and protein stability. Cell Commun Signal 19:27. https://doi.org/10.1186/s12964-020-00703-w

Rogers EM, Allred SC, Peifer M (2021b) Abelson kinase's intrinsically disordered region plays essential roles in protein function and protein stability. Cell Commun Signal 19:27. https://doi.org/10.1186/s12964-020-00703-w

Saiardi A (2004) Phosphorylation of Proteins by Inositol Pyrophosphates. Science (80-) 306:2101–2105. https://doi.org/10.1126/science.1103344

Saiardi A, Erdjument-Bromage H, Snowman AM, et al (1999) Synthesis of diphosphoinositol pentakisphosphate by a newly identified family of higher inositol polyphosphate kinases. Curr Biol 9:1323–1326. https://doi.org/https://doi.org/10.1016/S0960-9822(00)80055-X

Saiardi A, Qiu D, Eisenbeis VB, Jessen HJ (2021) Absolute Quantitation of Inositol Pyrophosphates by Capillary Electrophoresis Electrospray Ionization Mass Spectrometry. JoVE e62847. https://doi.org/doi:10.3791/62847

Sanchez AM, Garg A, Shuman S, Schwer B (2019) Inositol pyrophosphates impact

phosphate homeostasis via modulation of RNA 3’ processing and transcription termination. Nucleic Acids Res 47:8452–8469. https://doi.org/10.1093/nar/gkz567

Shears SB (2015) Inositol pyrophosphates: why so many phosphates? Adv Biol Regul 57:203–216. https://doi.org/10.1016/j.jbior.2014.09.015

Shukla A, Kaur M, Kanwar S, et al (2021) Wheat inositol pyrophosphate kinase TaVIH2-3B modulates cell-wall composition and drought tolerance in Arabidopsis. BMC Biol 19:261. https://doi.org/10.1186/s12915-021-01198-8

Thota SG, Bhandari R (2015) The emerging roles of inositol pyrophosphates in eukaryotic cell physiology. J Biosci 40:593–605. https://doi.org/10.1007/s12038-015-9549-x

Ward JJ, Sodhi JS, McGuffin LJ, et al (2004) Prediction and Functional Analysis of Native Disorder in Proteins from the Three Kingdoms of Life. J Mol Biol 337:635–645. https://doi.org/https://doi.org/10.1016/j.jmb.2004.02.002

Wilson MSC, Saiardi A (2017) Importance of Radioactive Labelling to Elucidate Inositol Polyphosphate Signalling. Top Curr Chem 375:14. https://doi.org/10.1007/s41061-016-0099-y

Wright PE, Dyson HJ (2015) Intrinsically disordered proteins in cellular signalling and regulation. Nat Rev Mol Cell Biol 16:18–29. https://doi.org/10.1038/nrm3920

Wu X, Lai Y, Lv L, et al (2020) Fasciclin-like arabinogalactan gene family in Nicotiana benthamiana: genome-wide identification, classification and expression in response to pathogens. BMC Plant Biol 20:305. https://doi.org/10.1186/s12870-020-02501-5

Yao K, Yao Y, Ding Z, et al (2023) Characterization of the FLA Gene Family in Tomato (Solanum lycopersicum L.) and the Expression Analysis of SlFLAs in Response to Hormone and Abiotic Stresses. Int J Mol Sci 24:. https://doi.org/10.3390/ijms242216063

Zang L, Zheng T, Chu Y, et al (2015) Genome-Wide Analysis of the Fasciclin-Like Arabinogalactan Protein Gene Family Reveals Differential Expression Patterns, Localization, and Salt Stress Response in Populus . Front. Plant Sci. 6

Zhou J, Hu Q, Xiao X, et al (2021) Mechanism of phosphate sensing and signaling revealed by rice SPX1-PHR2 complex structure. Nat Commun 12:7040. https://doi.org/10.1038/s41467-021-27391-5

Zhu J, Lau K, Puschmann R, et al (2019) Two bifunctional inositol pyrophosphate kinases/phosphatases control plant phosphate homeostasis. Elife 8:e43582. https://doi.org/10.7554/eLife.43582

Zsolt S, Assegid G, Cristina A, Adolfo S (2011) Influence of Inositol Pyrophosphates on Cellular Energy Dynamics. Science (80-) 334:802–805.

https://doi.org/10.1126/science.1211908

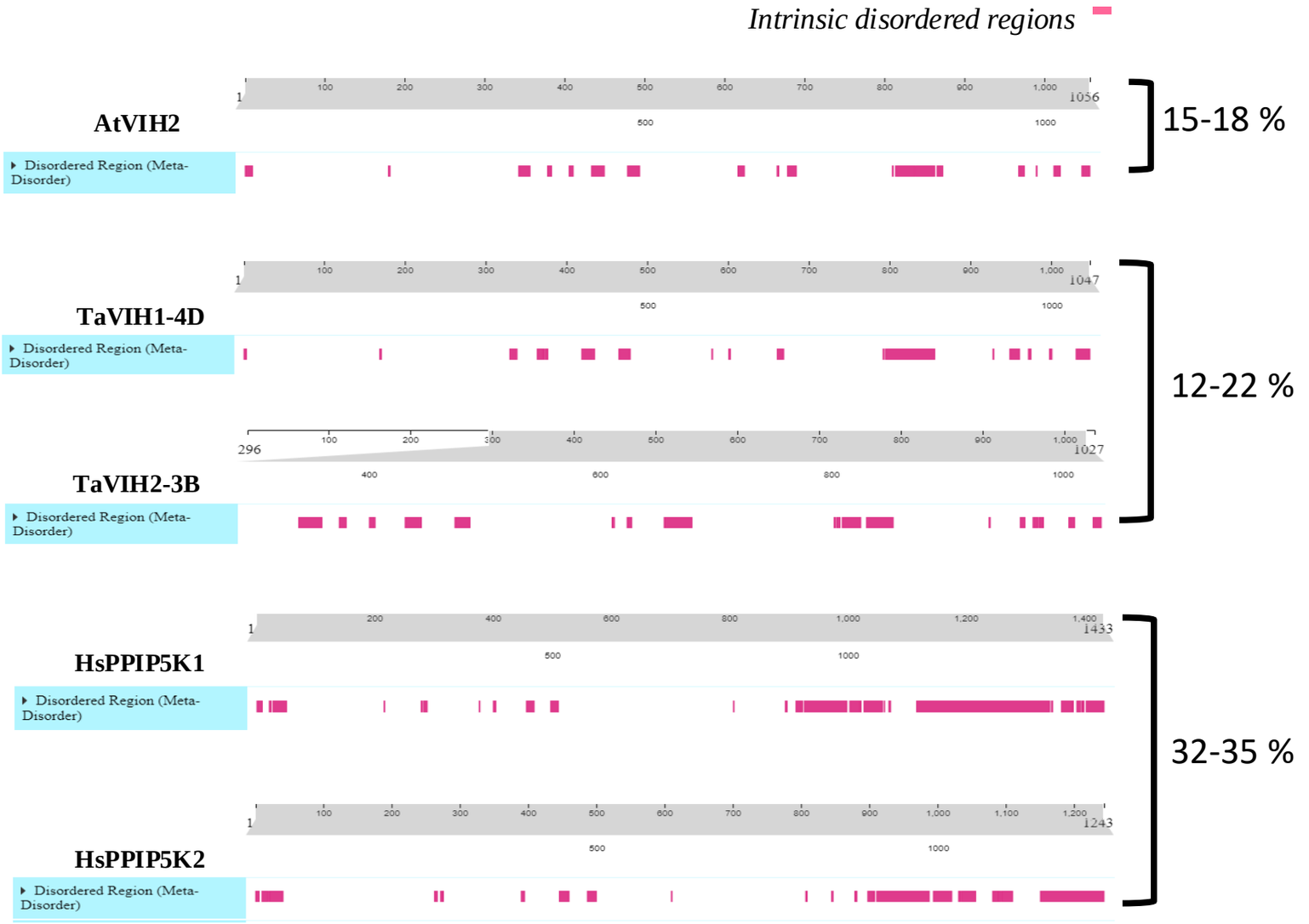
Intrinsic disordered regions
AtVIH2
Disordered Region (Meta-Disorder)
15-18 %
TaVIH1-4D
Disordered Region (Meta-Disorder)
TaVIH2-3B
Disordered Region (Meta-Disorder)
12-22 %
HsPPIP5K1
Disordered Region (Meta-Disorder)
HsPPIP5K2
Disordered Region (Meta-Disorder)
32-35 %

Figure 1

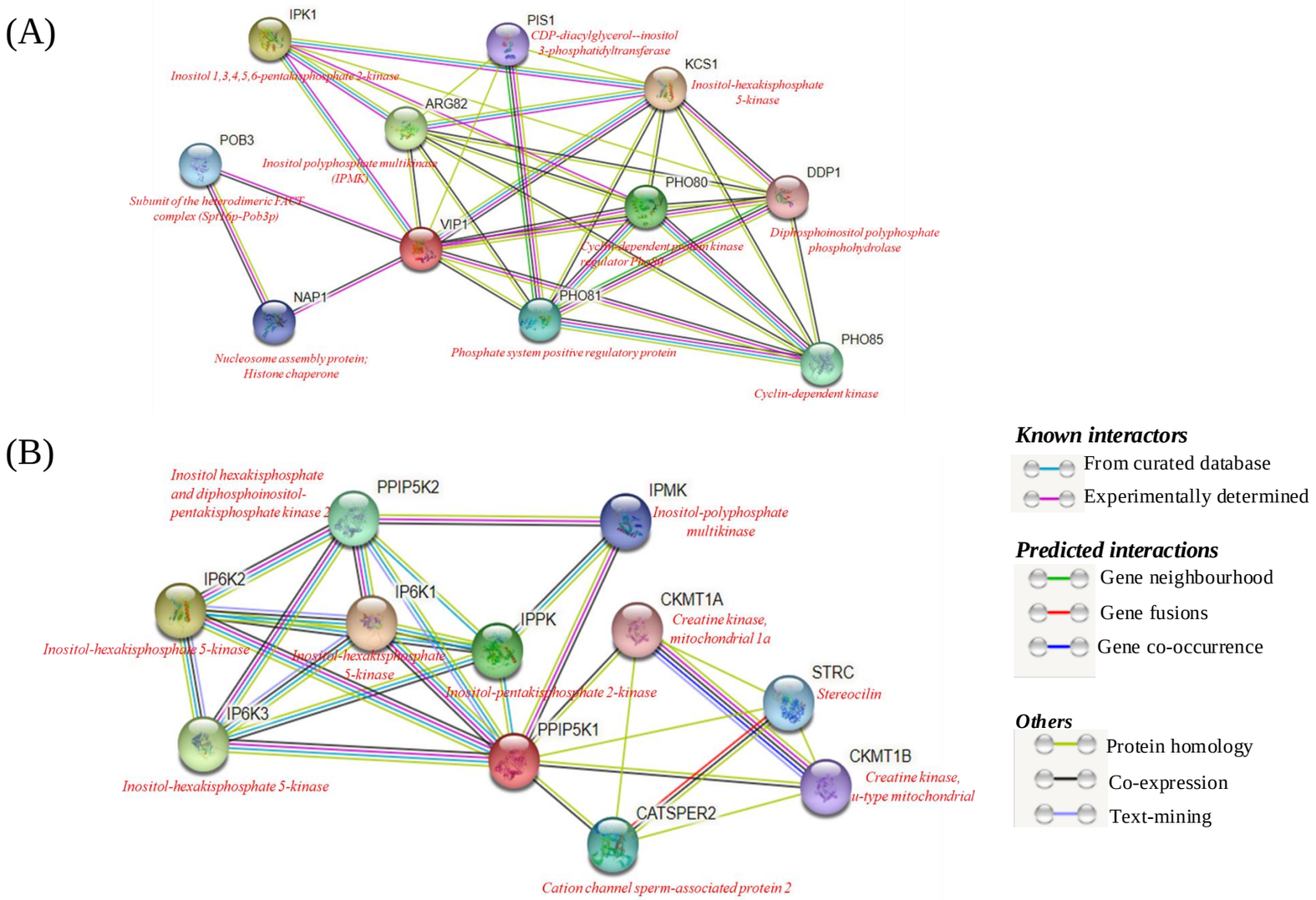
(A)
IPK1
Inositol 1,3,4,5,6-pentakisphosphate 2-kinase
PIS1
CDP-diacylglycerol--inositol 3-phosphatidyltransferase
KCS1
Inositol-hexakisphosphate 5-kinase
ARG82
Inositol polyphosphate multikinase (IPMK)
POB3
Subunit of the heterodimeric FACT complex (Spt16p-Pob3p)
PHO80
DDP1
Diphosphoinositol polyphosphate phosphohydrolase
VIP1
Cyclin-dependent protein kinase regulator Pho80
NAP1
Nucleosome assembly protein; Histone chaperone
PHO81
Phosphate system positive regulatory protein
PHO85
Cyclin-dependent kinase
(B)
Inositol hexakisphosphate and diphosphoinositol-pentakisphosphate kinase 2
PPIP5K2
IPMK
Inositol-polyphosphate multikinase
IP6K2
Inositol-hexakisphosphate 5-kinase
IP6K1
Inositol-hexakisphosphate 5-kinase
IPPK
Inositol-pentakisphosphate 2-kinase
CKMT1A
Creatine kinase, mitochondrial 1a
STRC
Stereocilin
IP6K3
Inositol-hexakisphosphate 5-kinase
PPIP5K1
CKMT1B
Creatine kinase, u-type mitochondrial
CATSPER2
Cation channel sperm-associated protein 2
Known interactors
From curated database
Experimentally determined
Predicted interactions
Gene neighbourhood
Gene fusions
Gene co-occurrence
Others
Protein homology
Co-expression
Text-mining
(C)
Traes_7AL_41C5592C4.1
Actin family protein
Traes_7BL_280BB2458.1
Actin family protein
Traes_2BL_A465A5769.1
ATP binding (GO:0005524), inositol pentakisphosphate 2-kinase activity (GO:0035299)
Traes_7BL_7DDF80D01.1
ATP binding (GO:0005524), inositol pentakisphosphate 2-kinase activity (GO:0035299)
Traes_6DL_B358A03CA.1
Actin family protein
Traes_3B_3567813F3.1
Traes_7DL_B6A7F350D.1
ATP binding (GO:0005524), inositol pentakisphosphate 2-kinase activity (GO:0035299)
Traes_6BL_033E8282D.2
Actin family protein
Traes_2AL_55460AE54.1
ATP binding (GO:0005524), inositol pentakisphosphate 2-kinase activity (GO:0035299)
Traes_6AL_7DF57A1F6.3
Actin family protein
Traes_2DL_EFEF40224.1
ATP binding (GO:0005524), inositol pentakisphosphate 2-kinase activity (GO:0035299)

Figure 2

(A)

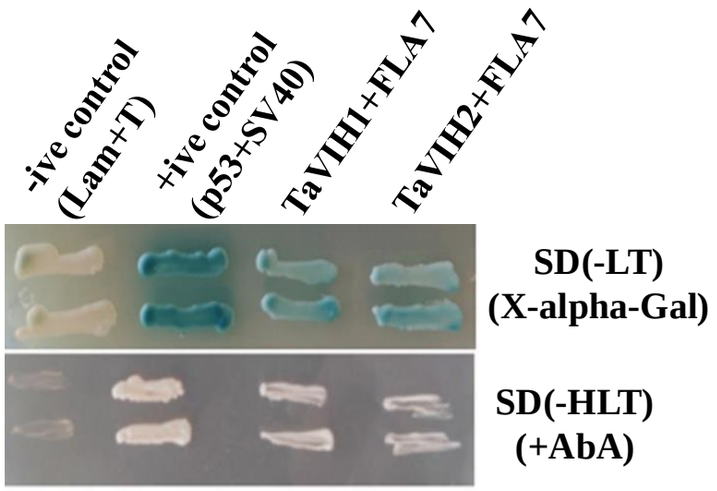
-ive control
(Lam+T)
+ive control
(p53+SV40)
TaVIH1+FLA7
TaVIH2+FLA7
SD(-LT)
(X-alpha-Gal)
SD(-HLT)
(+AbA)

(B)

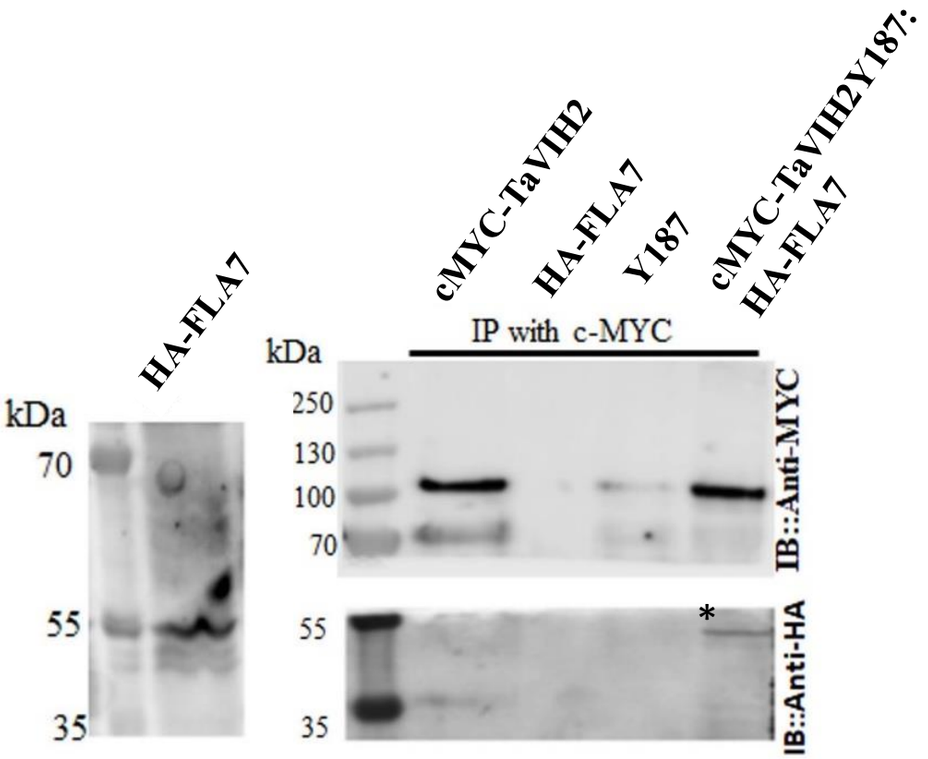
HA-FLA7
kDa
70
55
35
cMYC-TaVIH2
HA-FLA7
Y187
cMYC-TaVIH2Y187:
HA-FLA7
IP with c-MYC
kDa
250
130
100
70
55
35
*
IB::Anti-MYC
IB::Anti-HA

Figure 3

(A)

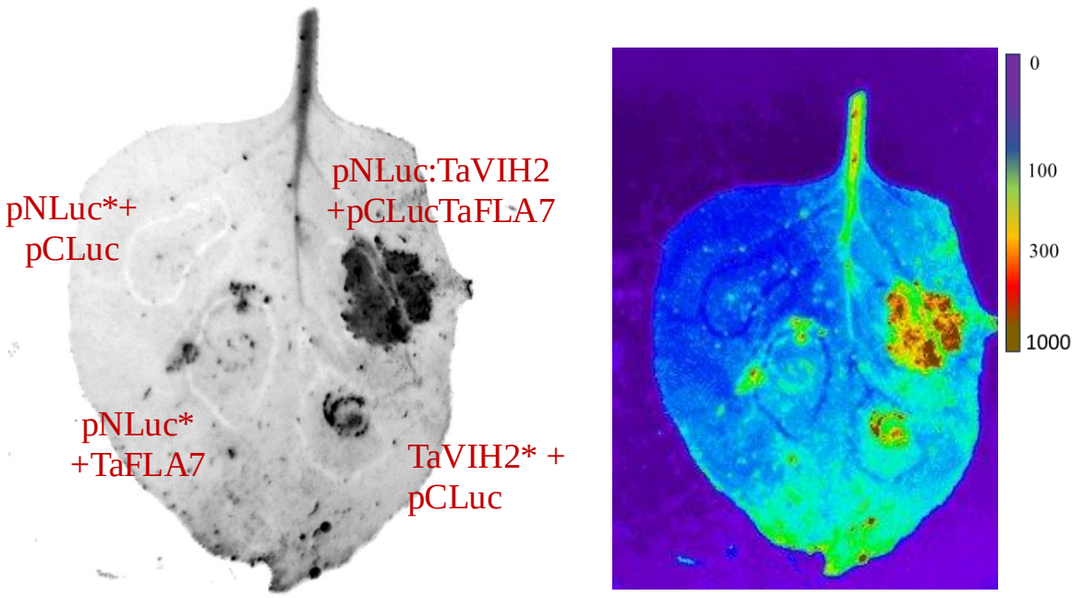
pNLuc*+
pCLuc
pNLuc:TaVIH2
+pCLucTaFLA7
pNLuc*
+TaFLA7
TaVIH2* +
pCLuc
0
100
300
1000

(B)

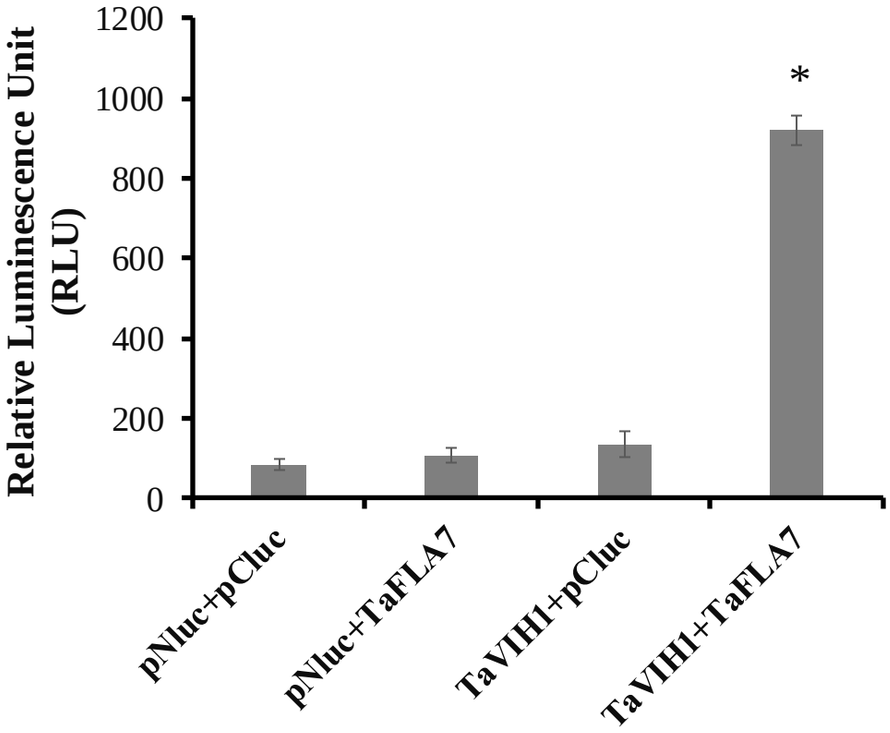
Relative Luminescence Unit
(RLU)
1200
1000
800
600
400
200
0
*
pNluc+pCluc
pNluc+TaFLA7
TaVIH1+pCluc
TaVIH1+TaFLA7

Figure 4

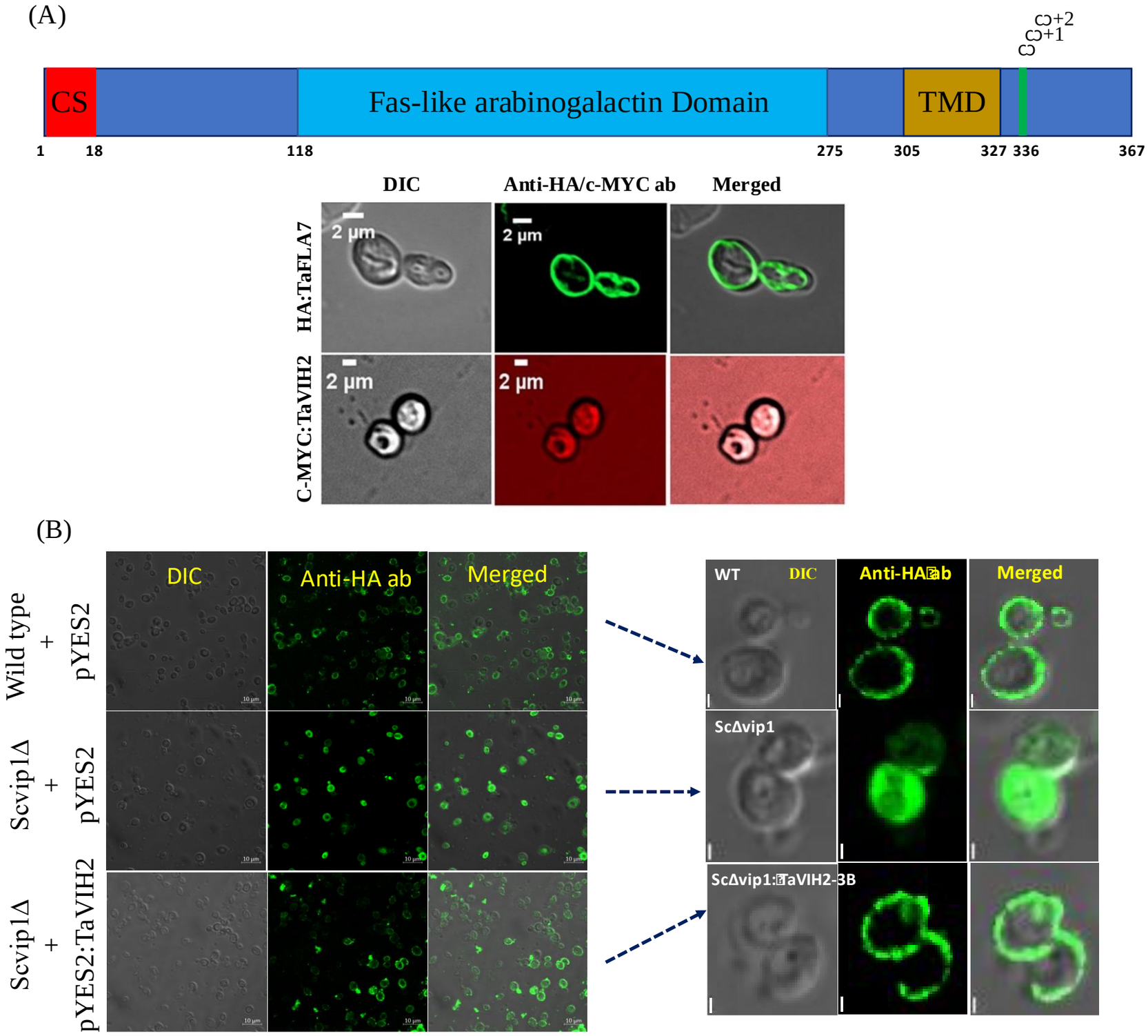
(A)
CS
Fas-like arabinogalactin Domain
TMD
CS+2
CS+1
CS
1
18
118
275
305
327
336
367
DIC
Anti-HA/c-MYC ab
Merged
HA:TaFLA7
C-MYC:TaVIH2
2 µm
(B)
Wild type + pYES2
Scvip1Δ + pYES2
Scvip1Δ + pYES2:TaVIH2
DIC
Anti-HA ab
Merged
WT
ScΔvip1
ScΔvip1:TaVIH2-3B

Figure 5

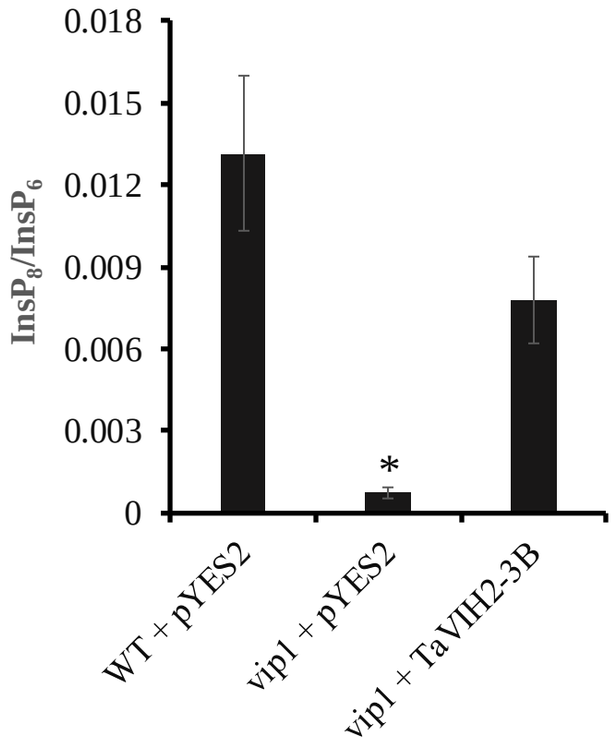
0.018
0.015
0.012
0.009
0.006
0.003
0
InsP8/InsP6
*
WT + pYES2
vip1 + pYES2
vip1 + TaVIH2-3B

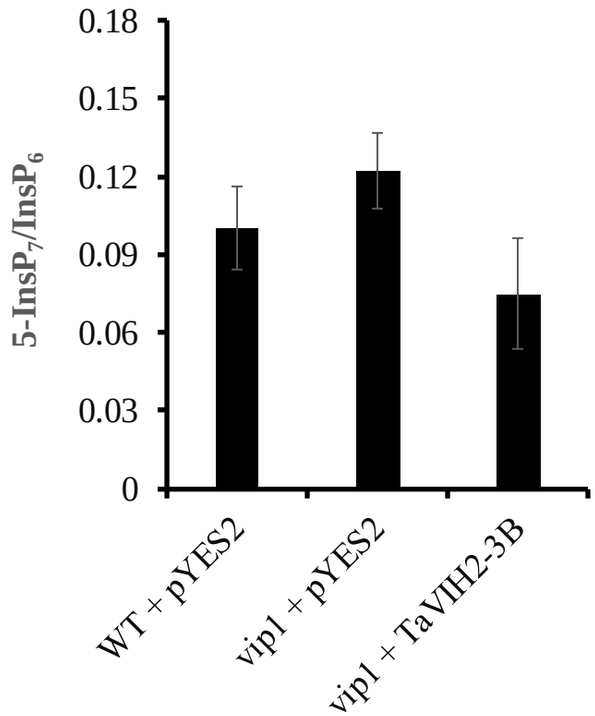
0.18
0.15
0.12
0.09
0.06
0.03
0
5-InsP7/InsP6
WT + pYES2
vip1 + pYES2
vip1 + TaVIH2-3B

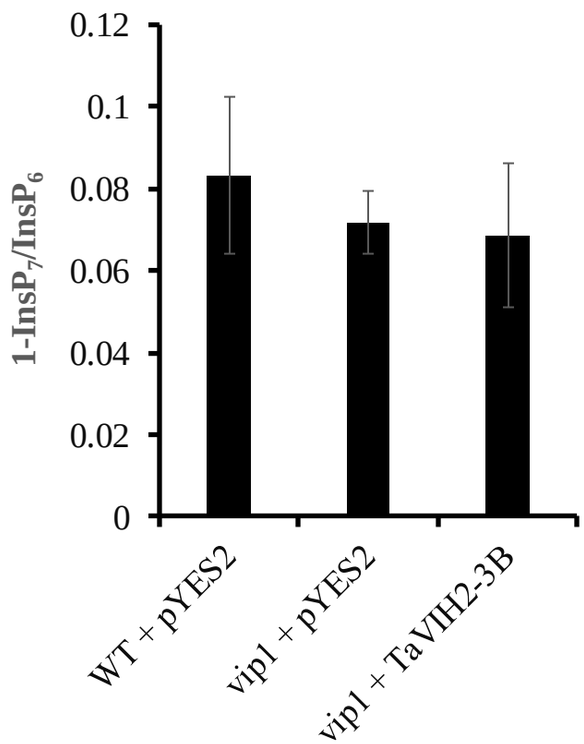
0.12
0.1
0.08
0.06
0.04
0.02
0
1-InsP7/InsP6
WT + pYES2
vip1 + pYES2
vip1 + TaVIH2-3B

Figure 6

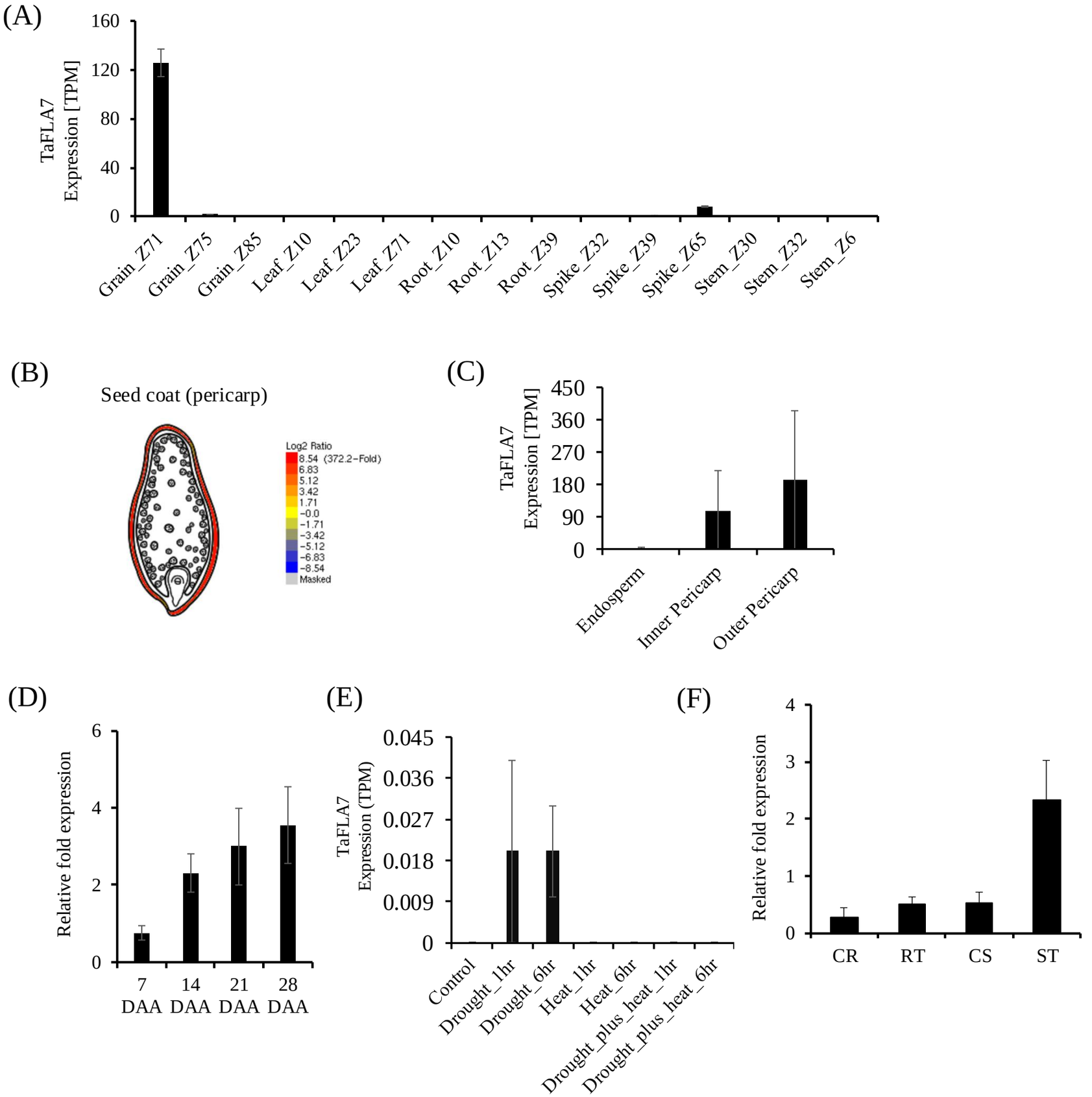
(A)
TaFLA7 Expression [TPM]
160
120
80
40
0
Grain_Z71
Grain_Z75
Grain_Z85
Leaf_Z10
Leaf_Z23
Leaf_Z71
Root_Z10
Root_Z13
Root_Z39
Spike_Z32
Spike_Z39
Spike_Z65
Stem_Z30
Stem_Z32
Stem_Z6
(B)
Seed coat (pericarp)
Log2 Ratio
8.54 (372.2-Fold)
6.83
5.12
3.42
1.71
-0.0
-1.71
-3.42
-5.12
-6.83
-8.54
Masked
(C)
TaFLA7 Expression [TPM]
450
360
270
180
90
0
Endosperm
Inner Pericarp
Outer Pericarp
(D)
Relative fold expression
6
4
2
0
7 DAA
14 DAA
21 DAA
28 DAA
(E)
TaFLA7 Expression (TPM)
0.045
0.036
0.027
0.018
0.009
0
Control
Drought_1hr
Drought_6hr
Heat_1hr
Heat_6hr
Drought_plus_heat_1hr
Drought_plus_heat_6hr
(F)
Relative fold expression
4
3
2
1
0
CR
RT
CS
ST

Figure 7

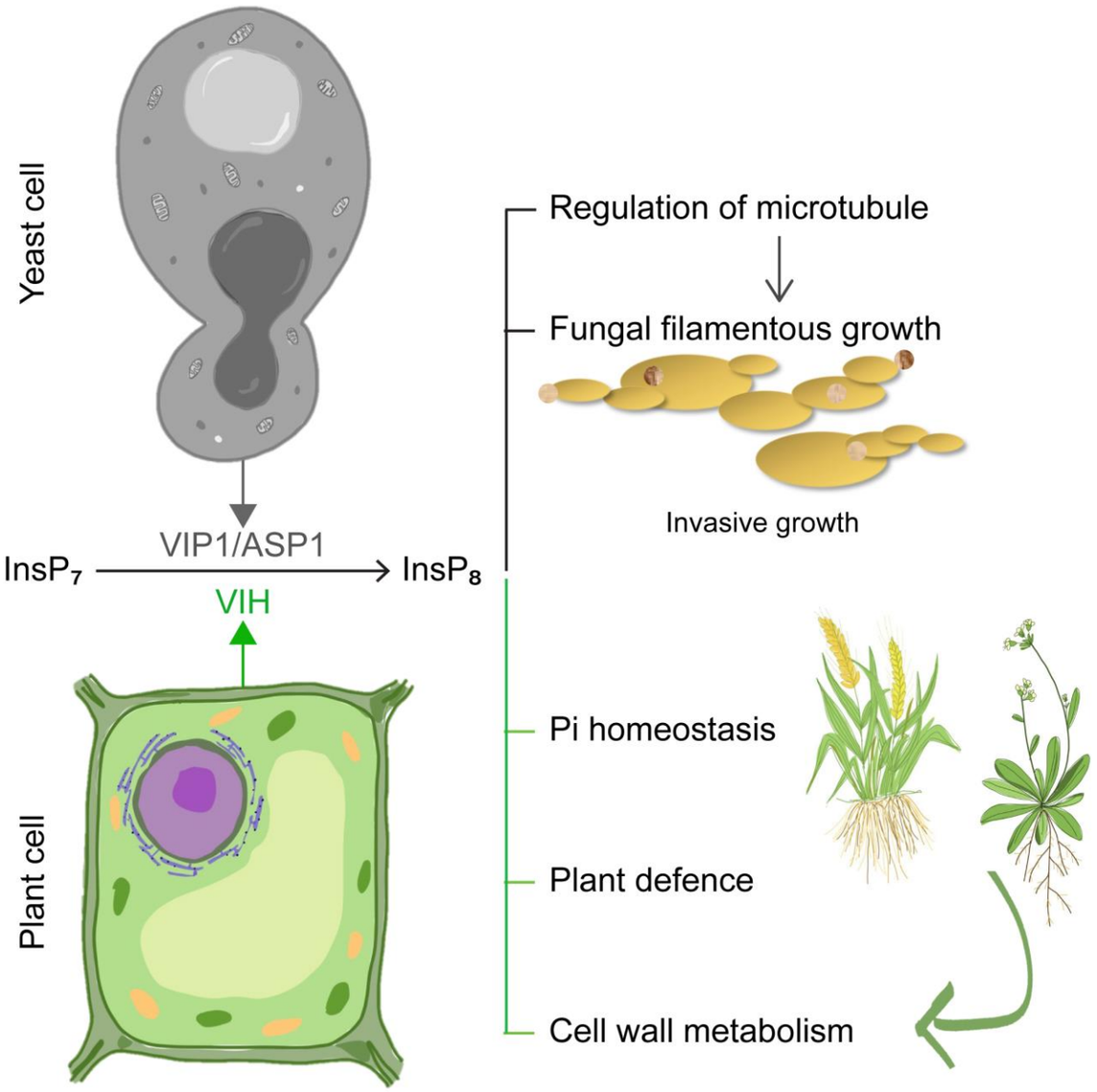
Yeast cell
VIP1/ASP1
InsP7
InsP8
VIH
Plant cell
Regulation of microtubule
Fungal filamentous growth
Invasive growth
Pi homeostasis
Plant defence
Cell wall metabolism

Figure 8